Statistical analysis of APXS-derived chemistry of the clay-bearing Glen Torridon region and the Mount Sharp group, Gale crater, Mars

Catherine Deborah O'Connell-Cooper[1], Lucy M. Thompson[1], John G. Spray[1]. Jeffrey A. Berger[2], Ralf Gellert[3], Michael McCraig[3], Scott J. VanBommel[4], Albert Yen[5]

[1]Planetary and Space Science Centre, University of New Brunswick, Fredericton, Canada

[2]NASA Johnson Space Center, Houston, TX, USA

[3]University of Guelph, Ontario, Canada

[4]Washington University, St. Louis, MO, USA

[5]Jet Propulsion Laboratory, California Institute of Technology, Pasadena, CA, USA

Contents of this file
> Text S1 to S2
> Figures S1 to S11
> Table Captions S1 to S7

Additional Supporting Information (Files uploaded separately)
Tables S1-S7 uploaded as a single Excel file:
Table S1. APXS compositional data for all targets, including location information, errors and operational statistics
Table S2. Mean values for Glen Torridon subunits and facies
Table S3. Pearson correlation coeffience (r), univariate analysis for all data.
Table S4 Variance analysis, incorporating all targets included mean Murray and Carolyn Shoemaker formations (n targets=488).
Table S5. Jura member (GT & VRR) subunits, AHCA, variance analysis results.
Table S6. Knockfarrill Hill member subunits, AHCA and variance analysis results
Table S7. Glasgow member subunits, AHCA and variance analysis results.

Introduction

Text S1. APXS instrumentation

Text S2. Statistical analysis – derivation of mean Murray and Carolyn Shoemaker formation (mean Mf+CSf); Agglomerative Hierarchical Clustering analysis (AHCA) models.

Figure S1 includes stratigraphic column for Gale crater, Mars and a localization map of showing Glen Torridon drill target locations and Mars Hand Lens Imager (MAHLI) images

Figure S2 shows examples of morphological expression of the Jura member in Glen Torridon, (Jm_GT), Murray formation, and includes both Mastcam and Mars Hand Lens Imager (MAHLI) images.

Figure S3 shows examples of morphological expression of the Knockfarril Hill member, Carolyn Shoemaker formation and includes both Mastcam and Mars Hand Lens Imager (MAHLI) images.

Figure S4 shows examples of morphological expression of the Glasgow member, Carolyn Shoemaker formation, using Mastcam images.

Figure S5 shows examples of diagenetic features within the Hutton interval of the Glasgow member, Carolyn Shoemaker formation and includes both Mastcam and Mars Hand Lens Imager (MAHLI) images.

Figure S6 shows examples of diagenetic features in the Glasgow member, Carolyn Shoemaker formation and using Mars Hand Lens Imager (MAHLI) images.

Figure S7 shows change in concentrations, with increasing elevation, relative to mean Murray and Carolyn Shoemaker formations.

Figure S8 (a-d) summarizes the results of Agglomerative Hierarchical Clustering analysis for the Jura member within Glen Torridon, for all three models (models discussed in Supplementary Text S2b).

Figure S9 compares the Jura member within Glen Torridon (Jm_GT) to that on Vera Rubin ridge (Jm_VRR), using multivariate Principal component analysis (PCA).

Figure S10 (a-d) summarizes the results of Agglomerative Hierarchical Clustering analysis for the Knockarril Hill member, for all three models (models discussed in Supplementary Text S2b).

Figure S11 (a-d) summarizes the results of Agglomerative Hierarchical Clustering analysis for the Glasgow member, for all three models (models discussed in Supplementary Text S2b).

Text S1.

The Mars Science Laboratory (MSL) Alpha particle X-ray Spectrometer (APXS):
The MSL APXS combines particle-induced X-ray emission (PIXE) and X-ray fluorescence (XRF) to analyze rock and unconsolidated sediment targets for major elements from Z=11 to 26 (Na, Mg, Al, Si, P, S, Cl, K, Ca, Ti, Cr, Mn, Fe) and trace elements (Ni, Zn, Br, Ge, Cu, Se, As, Pb. Ga, Rb, Sr, Y, W and Pb). PIXE is efficient at exciting lower atomic numbers and XRF those with higher atomic numbers [*Gellert et al.,* 2006].
APXS consists of a main electronics unit in the rover's body and a sensor head, with six ^{224}curium radionuclide sources concentrically surrounding a silicon drift detector, mounted on the robotic arm [*Gellert et al.*, 2006]. To analyze a sample, the sensor head is placed on (in contact) or close to ("hovering") the target, for a period of time ranging from 20 minutes to eight hours. Distance from the sample increases the "field of view" (FOV) from the nominal ≈ 15 mm diameter [*Gellert et al.*, 2015; *VanBommel et al.*, 2016, 2017]. The sample is irradiated with alpha particles and X-ray radiation, resulting in the generation of X-rays with specific energies for each element, producing a spectrum. Observed elemental data are converted into standard oxide data using a specially developed data analysis technique ("Gellert method", originally developed for the MER APXS), by fitting summed spectra into a non-linear least squares fit routine [described in *Gellert et al.*, 2006]. The fitting procedure results in peak areas of the characteristic element lines, which are first converted into element and then into oxide concentrations (using calibration tables). The oxide sum (geometric norm) is renormalized to 100% to compensate for the unknown distance of the sensor head to the sample surface, and allow for distance dependent corrections for elemental background contributions [*Gellert et al.*, 2006]. The final output of the analysis consists of elemental concentrations (in weight percent), and their 2-sigma statistical error, which represent the precision of the data. Current best estimates for overall analytical accuracy, determined by comparison with a suite of geochemical reference materials: ±3 % (relative) for Si; ±7-% Al, Ca, Fe; ±7 % Mn; ±11 % Na; ±14 % Mg; ±15 % P, S, K; ±16 % for Ni, Zn; ±19 % Cr; ±11 %; ±20 % Ti, Br; ±30 % for Cl [*Gellert et al.*, 2006]. Instrument performance is monitored by periodically calibrating to an on-board basaltic calibration slab ("BT-2") [*Campbell et al.*, 2012; *Thompson et al.*, 2012, 2013].

Text S2.

S2a. Arithmetic mean Murray and Carolyn Shoemaker formation

The arithmetic mean for Murray and Carolyn Shoemaker formation (**mean Mf=CSf**) (Tables 2a, S1) was compiled from 488 representative bedrock and drill fines targets, across the nine members included at time of writing:

Glasgow mbr (Gm), Carolyn Shoemaker fm [Fedo et al., this issue]
Knockfarril Hill mbr (KHm), Carolyn Shoemaker fm [Fedo et al., this issue, 2020]
Jura member (Jm), Murray fm [Edgar et al., 2020]
Pettegrove Point member (PPm), Murray fm [Edgar et al., 2020]
Blunts Point member (BPm), Murray fm [Fedo et al., 2019]
Sutton Island member (SIm), Murray fm [Fedo et al., 2019]
Karasburg member (KBm), Murray fm [Fedo et al., 2019]
Hartmanns's Valley member (HVm), Murray fm [Fedo et al., 2019]
Pahrump Hills member (PHm), Murray fm [Fedo et al., 2019]

Column D, Table S1, indicates targets included in the mean. Targets were identified as outliers using standard (Z) scores to identify targets outside of the 95% confidence interval (±1.96 Standard Error). These samples were then investigated individually, via Mars Hand Lens Imager (MAHLI) images etc. Targets excluded: rubble-sand mixed regolithic targets in Glen Torridon, which often have a degree of sand or soil contributing to the target composition; obvious vein targets; targets with combined $CaO+SO_4$ > 20 wt. %; targets with high SiO_2 (> 65 wt. %, typically associated with zones of alteration at Marias Pass [Yen et al., 2017; Frydenvang et al. 2017]; all Hutton interval targets; diagenetic features such as concretions and nodules, including those with MnO >0.75 wt% and P_2O_5 >1.95 wt.%; targets with FWHM ≥200 eV.

S2b. Agglomerative Hierarchical Clustering analysis (AHCA):

AHCA was run to investigate similarities within members (Jm_GT, Section 4.1.2; KHm, Section 4.2.2; Gm Section 4.3.2; Jm_GT and Jm_VRR, Section 5.1). The Euclidean distance metric was used for all models and Ward's minimum variance method was used to define cluster linkages as it defines with clusters with low internal dissimilarity. All data was in the form of Log_{10}[element/Si] mole ratios, to minimize closure issues, associated with normalizing APXS data to 100% [Gellert et al., 2006; Chayes, 1971; Aitchison, 1994]. Targets excluded obvious diagenetic features, sand, soil and regolithic measurements from across Glen Torridon, whose compositions may have included contributions from unconsolidated materials. Drill fines were initially included but plotted distinctly for the majority of models and excluded in later runs. The ideal cluster size (K) was determined through the sum of squares method ("elbow method").

For each data set, three model parameters were run. Model A includes all elements routinely reported on by APXS. Following Mittlefehldt et al. [2018, 2021], Model B excludes the volatile elements S, Cl, Br, to minimize the effect of such variable elements on the bedock clustering. Model C excludes S, Cl, Br and the mobile elements Mn, P, Zn, Ni to examine the extent of alteration [e.g., Mittlefehldt et al. 2018, 2021].
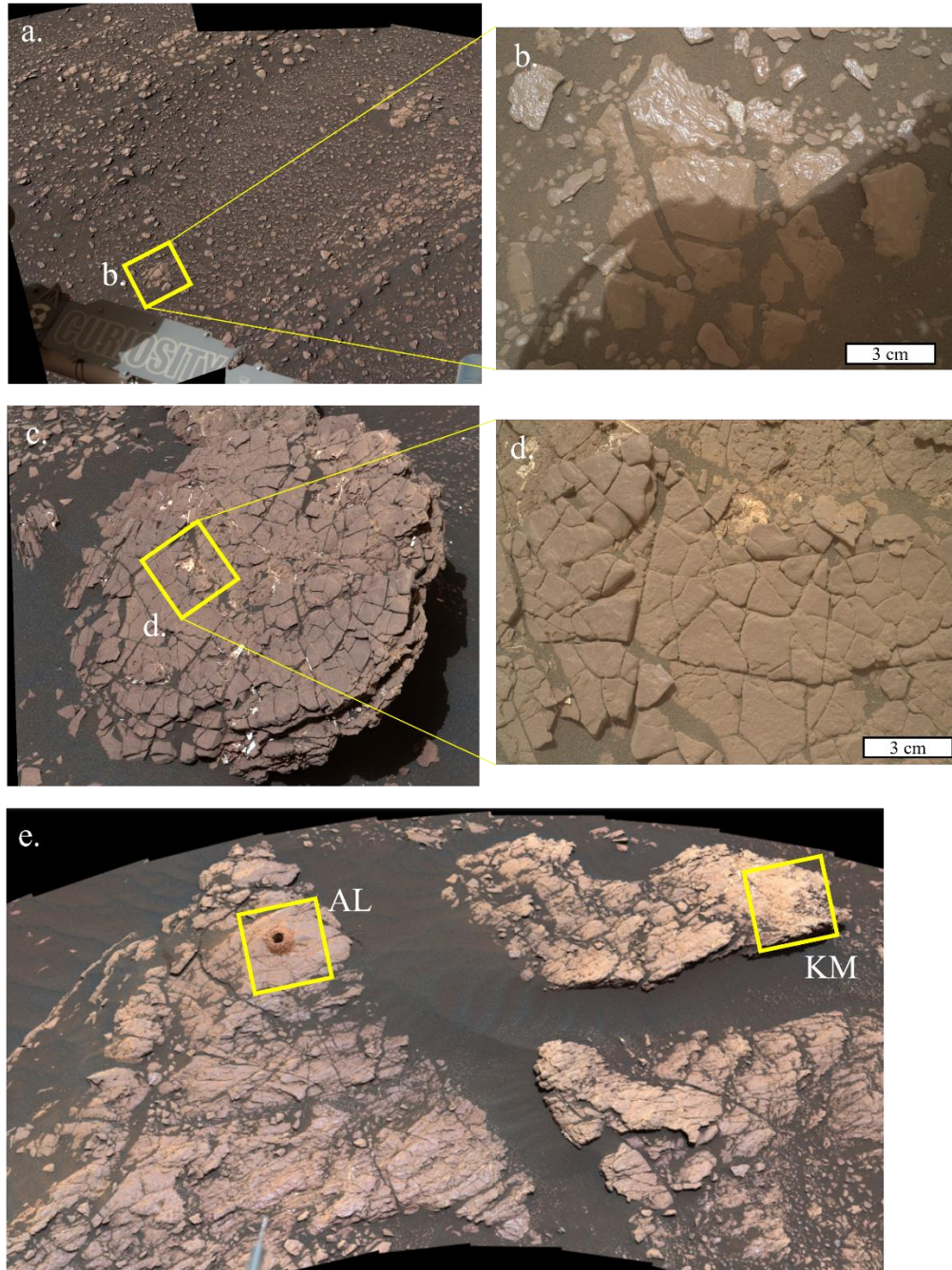
Figure S1. Map of Glen Torridon, Gale crater, Mars, showing drill target locations and images. **S1A.** Stratigraphic column [after *Fedo et al., this issue*], with study area highlighted in red. S1B. Localization map, showing drill target locations marked by red circles and official acronyms. Date of drill target acquisition is shown on insert images. Image S1B Courtesy of F. Calef III, and NASA/JPL-Caltech/MSSS/UofA/USGS-Flagstaff.

Figure S2. The Jura member in Glen Torridon, (Jm_GT), Murray (section 4.1.1). APXS target names are in italics, followed by sol of acquisition and Mastcam or Mars Hand Lens Imager (MAHLI) identifiers in brackets. Mastcam mosaic and MAHLI images: NASA/JPL-Caltech/MSSS. **S2a**. Typical regolithic, rubbly Jm_GT (Mastcam sequence 012509, sol 2361). **S2b**. *Ardmillan*, sol 2361 (2361MH0007060010804640C00). **S2c**. Muir of Ord boulder (Mastcam sequence 12474, sol 2352). **S2d**. *Crieff*, sol 2352 (2352MH0007060020804421C00). **S2e**. *Kilmarie* (KM) and *Aberlady* (AL) drill locale, coherent sandstone bedrock (Mastcam sequence 012571, sol 2371)..
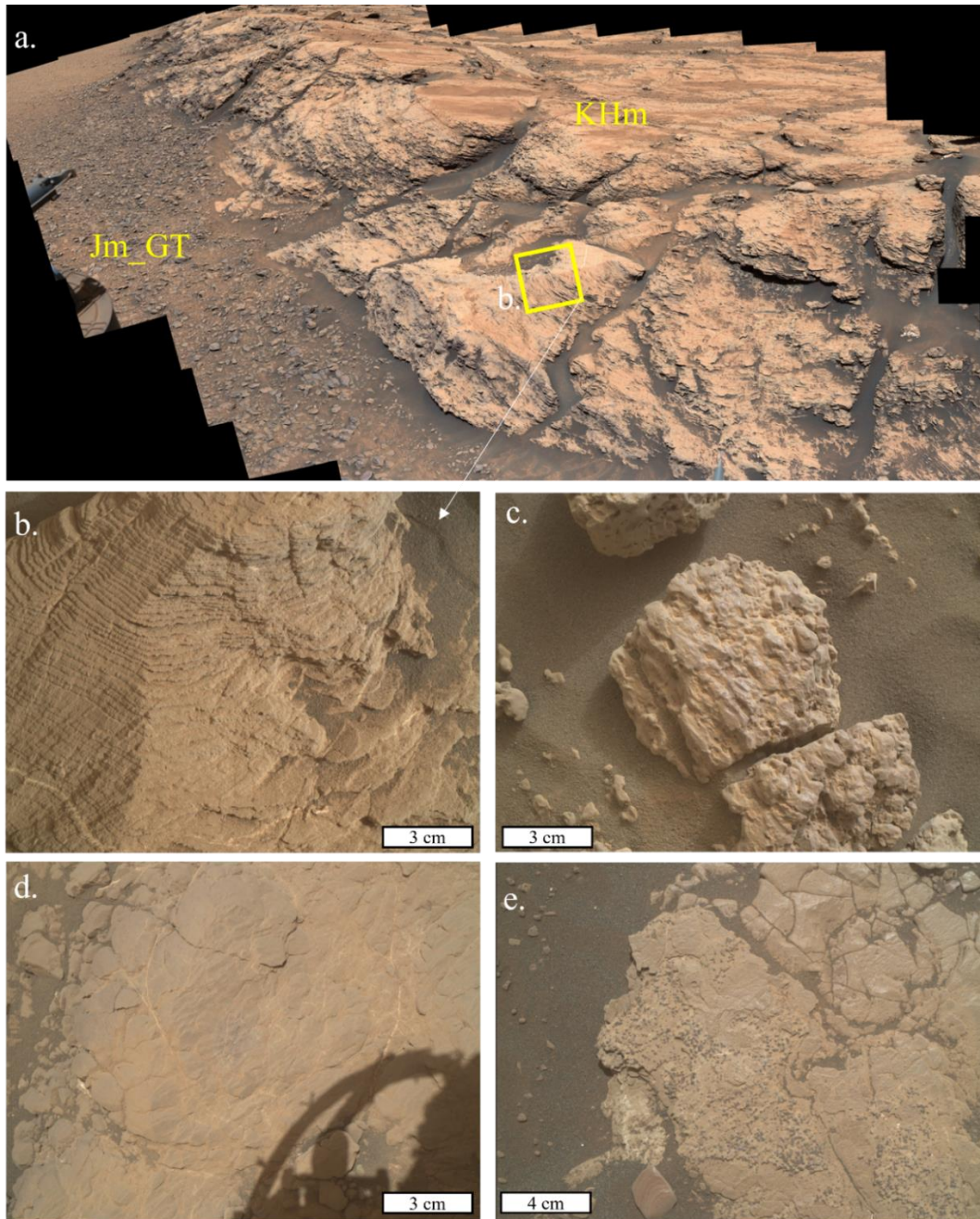
Figure S3. The Knockfarril Hill member, Carolyn Shoemaker formation (Section 4.2.1). APXS target names are in italics, followed by sol of acquisition and Mastcam or Mars Hand Lens Imager (MAHLI) identifiers in brackets. Mastcam mosaic and MAHLI images: NASA/JPL-Caltech/MSSS. **S3a**. Teal ridge, showing KHm sandstones overlying regolithic Jm_GT (Mastcam sequence 013416, sol 2553). **S3b**. *Balnakettle*, sol 2443 (2443MH0007060020901544C00). **S3c**. *Shetland*, sol 2564 (2564MH0001900010903636CO). **S3d**. *Nedd*, sol 2590 (MH0007060010904574C00). **S3e.** *Groken*, sol 2906 (2906MH0004240011003483C00).
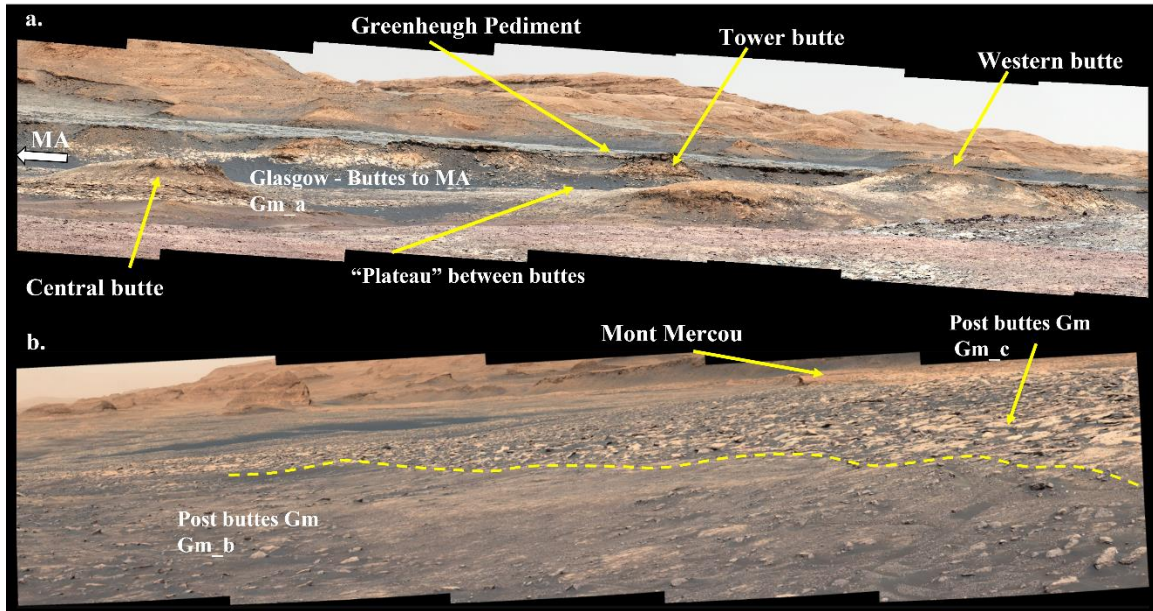
Figure S4. The Glasgow member, Carolyn Shoemaker formation (Section 4.3.1). Mastacam image identifiers are in brackets, with sol of acquisition. Mastcam mosaics: NASA/JPL-Caltech/MSSS. **S4a**. Mastcam mosaic (Mastcam sequence 013985, sol 2019) of the approach to Central, Western and Tower buttes, comprised of the main Glasgow member (Gm_a). The Hutton interval and drill locale is at the top of Tower butte, in contact with the overlying Greenheugh pediment. The Mary Anning drill locale is to the left of the buttes complex **S4b.** Approach to Mont Mercou, across the Glasgow member subunits Gm_b and Gm_c (Mastcam sequence 015740, sol 3018).
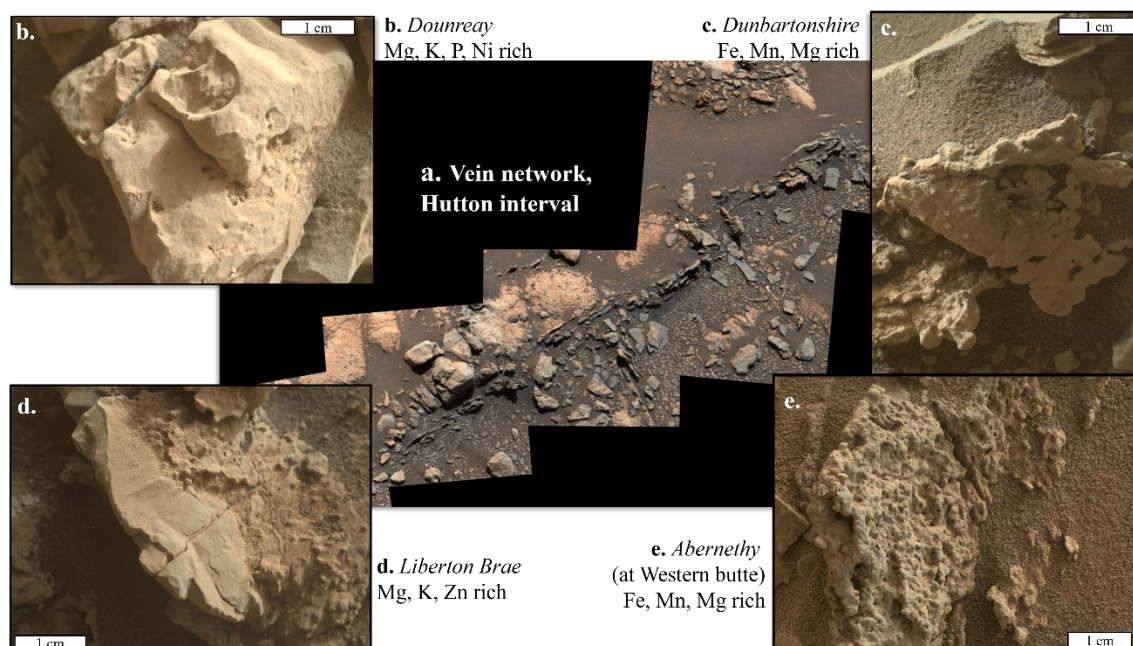
b. *Dounreay*
Mg, K, P, Ni rich

c. *Dunbartonshire*
Fe, Mn, Mg rich

a. Vein network, Hutton interval

d. *Liberton Brae*
Mg, K, Zn rich

e. *Abernethy*
(at Western butte)
Fe, Mn, Mg rich

Figure S5. Examples of diagenetic features within the Hutton interval, Glasgow member, Carolyn Shoemaker formation. APXS target names are in italics, followed by sol of acquisition and Mastcam or Mars Hand Lens Imager (MAHLI) identifiers in brackets. Mastcam mosaic and MAHLI images: NASA/JPL-Caltech/MSSS. **S5a**. Mastcam mosaic of a complex vein network within the Hutton interval, on Tower butte (Mastcam sequence 013985, sol 2666). **S5b-S5e**: All MAHLI images are from Tower butte, except S5e from Western butte. **S5b**. Dounreay, sol 2690 (2690MH0003060011001889C00). **S5c**. *Dunbartonshire*, sol 2690 (2690MH0001930001001912R00). **S5d**. *Liberton Brae*, sol 2666 (2666MH0002970011001579C00). **S5e**. *Abernethy*, sol 2642 (2643MH0004580001001002R00).
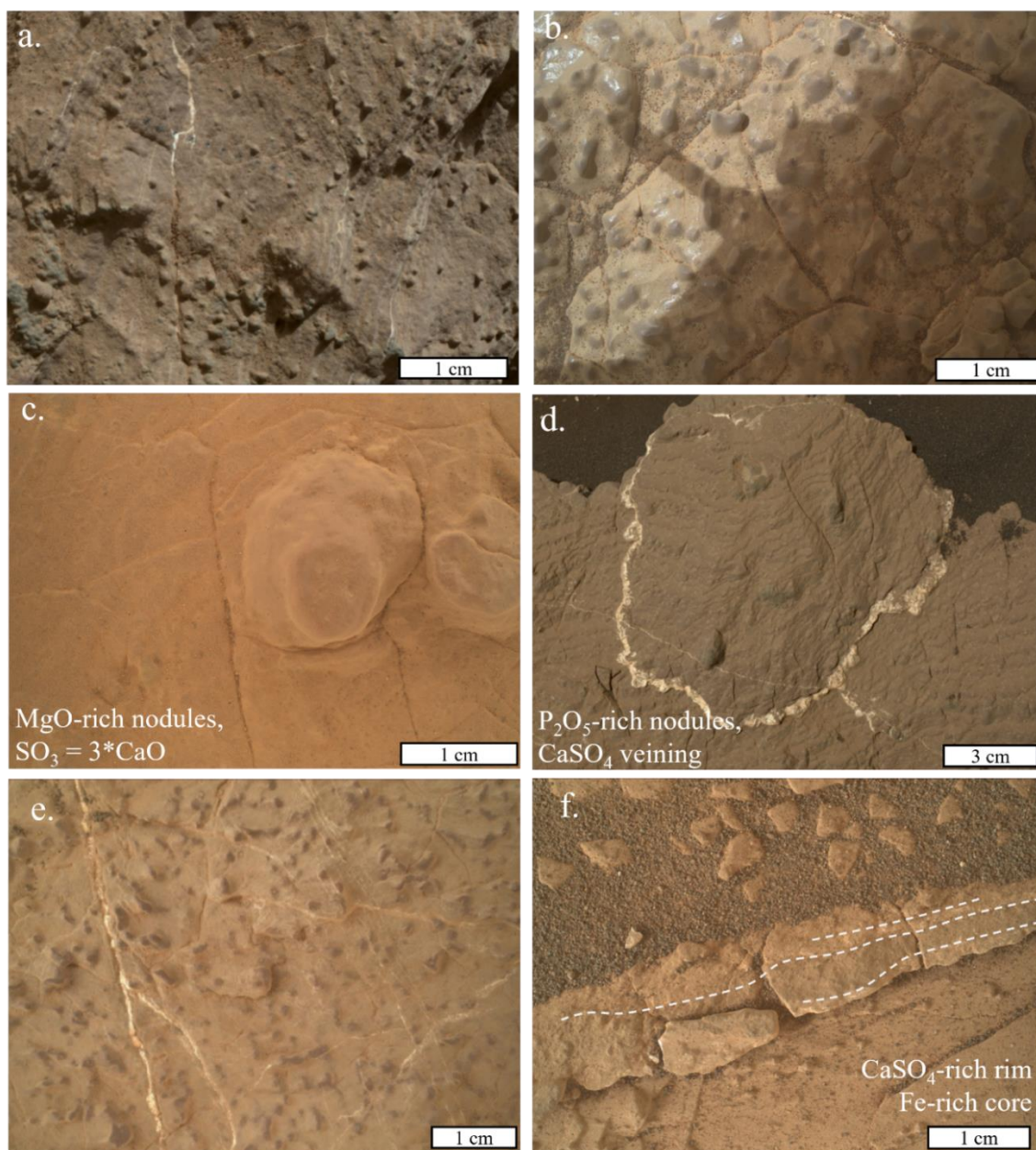
Figure S6. Examples of diagenetic features within the Glasgow member, Carolyn Shoemaker formation (Sections 4.3.1, 5.5). APXS target names are in italics, followed by sol of acquisition and or Mars Hand Lens Imager (MAHLI) identifiers in brackets. MAHLI images: NASA/JPL-Caltech/MSSS. **S6A**. *Sourhope*, sol 2583 (2583MH0001930000904258R00). **S6b**. *Achnasheen*, sol 2965 (2965MH0001820011004418C00). **S6c**. *An Dun*, sol 2974 (2974MH0001700000904677R00). **S6d**. *Beaupouyet*, sol 3015 (3015MH0007060011100271C00). **S6e**. *Limeyrat*, sol 3034 (3034MH0006990011100677C00). **S6f**. *Chassenon*, sol 3069 (3069MH0007630011101184C00).
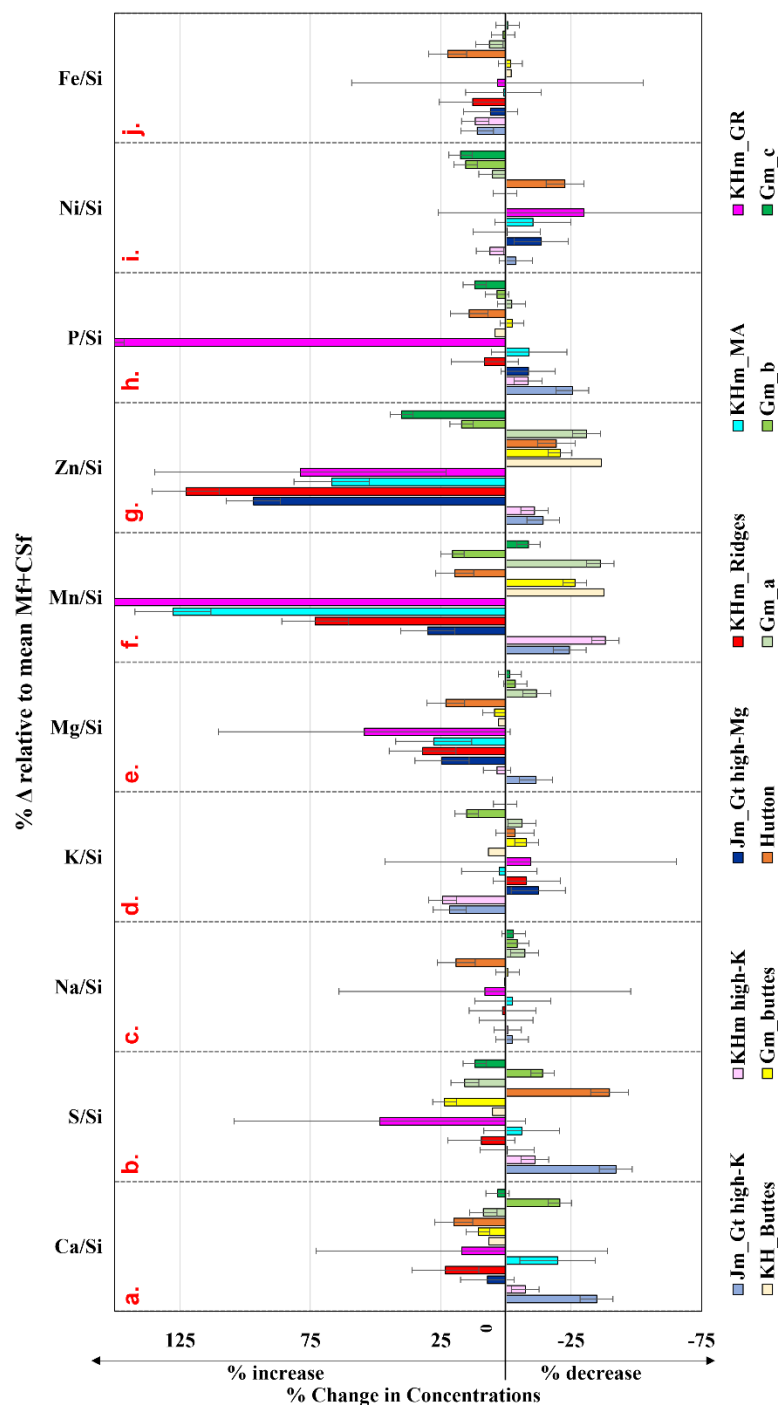
Figure S7. Changes in concentration, with increasing elevation, depicted as % change relative to mean Murray and Carolyn Shoemaker formations (Mf+CSf). All data in X/Si (molar) form. Each unit is shown in campaign order, except KHm_MA (shown next to other KHm units, and comparable elevations). KHm high-K unit = South Visionarium and traverse targets. KHm_Buttes and Gm_Buttes = targets from sols 2570 to 2653.

Jm_GT, Model A

Model A elements:

Ti, Al, Cr, Mn, Fe, Mg, Ca, Na, K, P, S, Cl, Ni, Zn, Br

Jm_GT, Model B

Model B elements:

Ti, Al, Cr, Mn, Fe, Mg, Ca, Na, K, P, Ni, Zn

Jm_GT, Model C

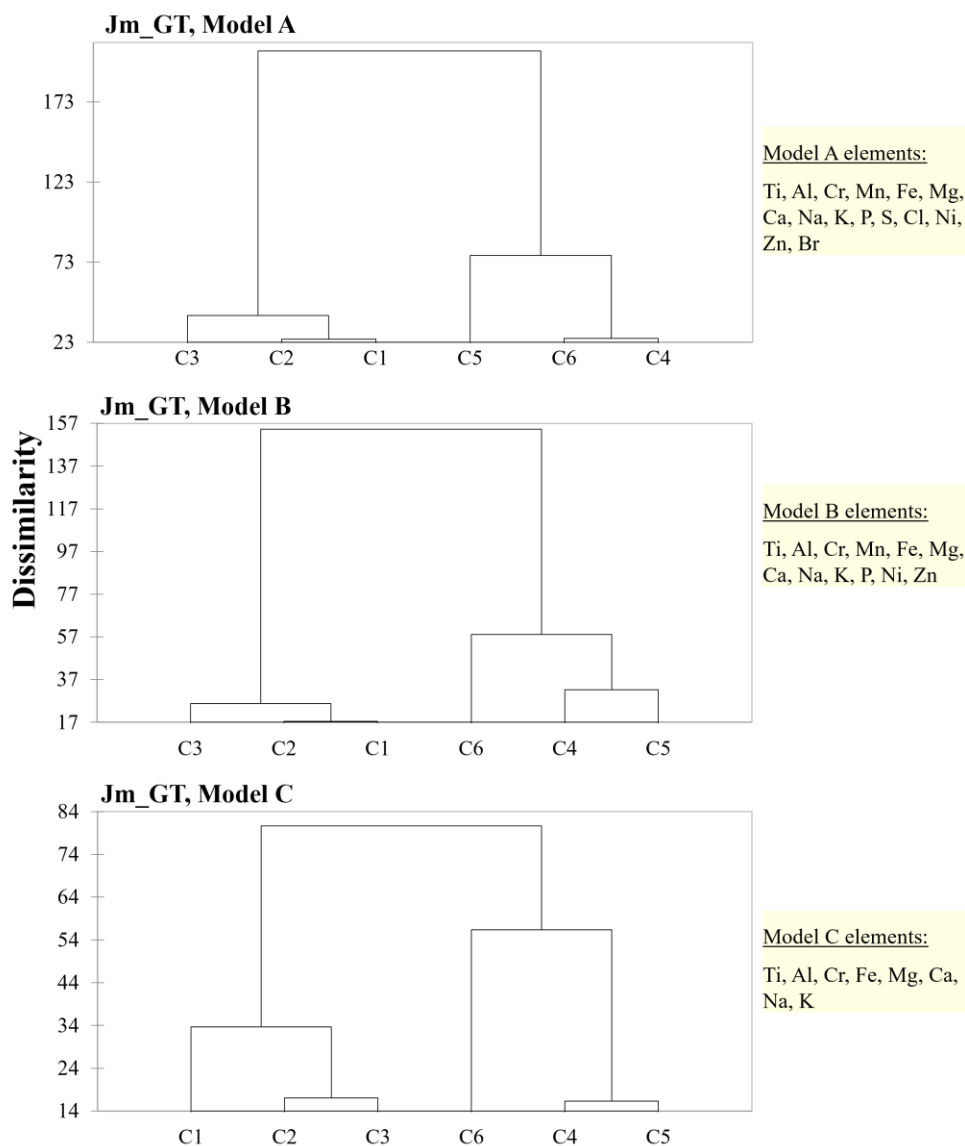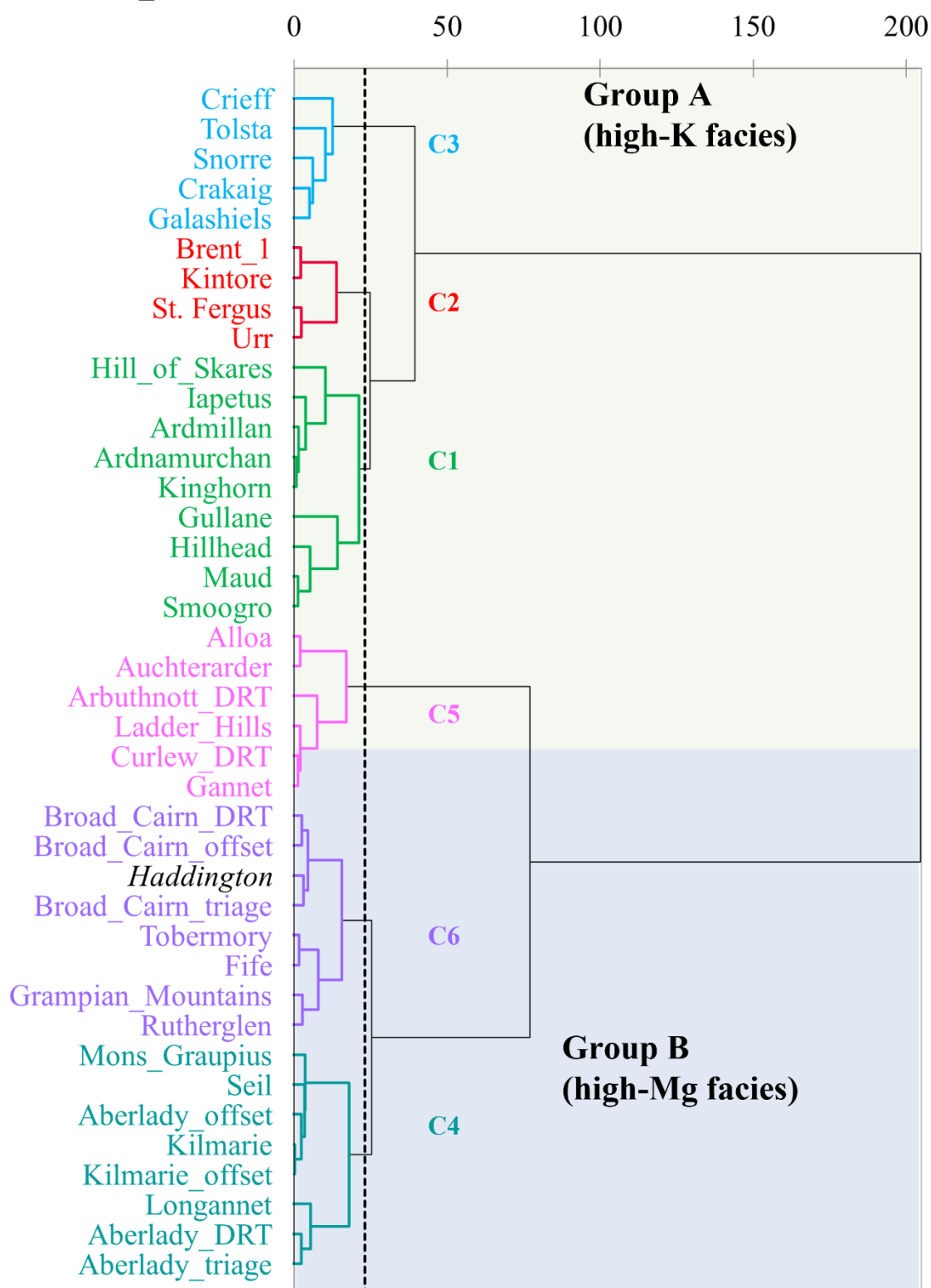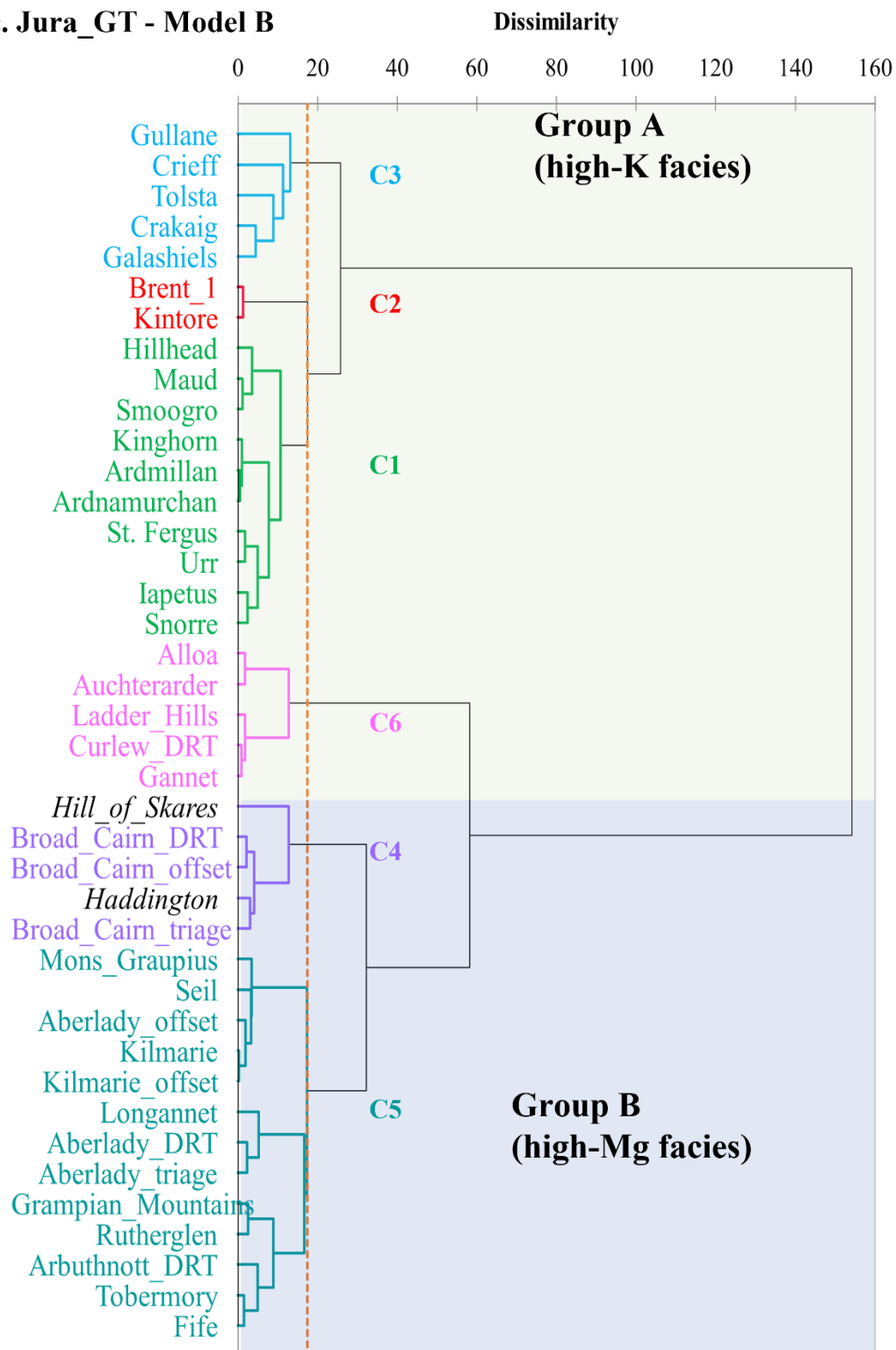Model C elements:

Ti, Al, Cr, Fe, Mg, Ca, Na, K

Figure S8. Agglomerative Hierarchical Clustering analysis (AHCA) dendrograms for Jura member (Glen Torridon) (n targets = 40). All models were run using Log10 (element/Si) (mole ratios). Model parameters are discussed in Section 3.3 and Supplementary Text S2b; results are listed in Table S5a and discussed in Section 4.1.2. **S8a.** Comparison of dendrograms for Models A-C, with detailed views for each model (with target names in figures **S8b-S8d**.
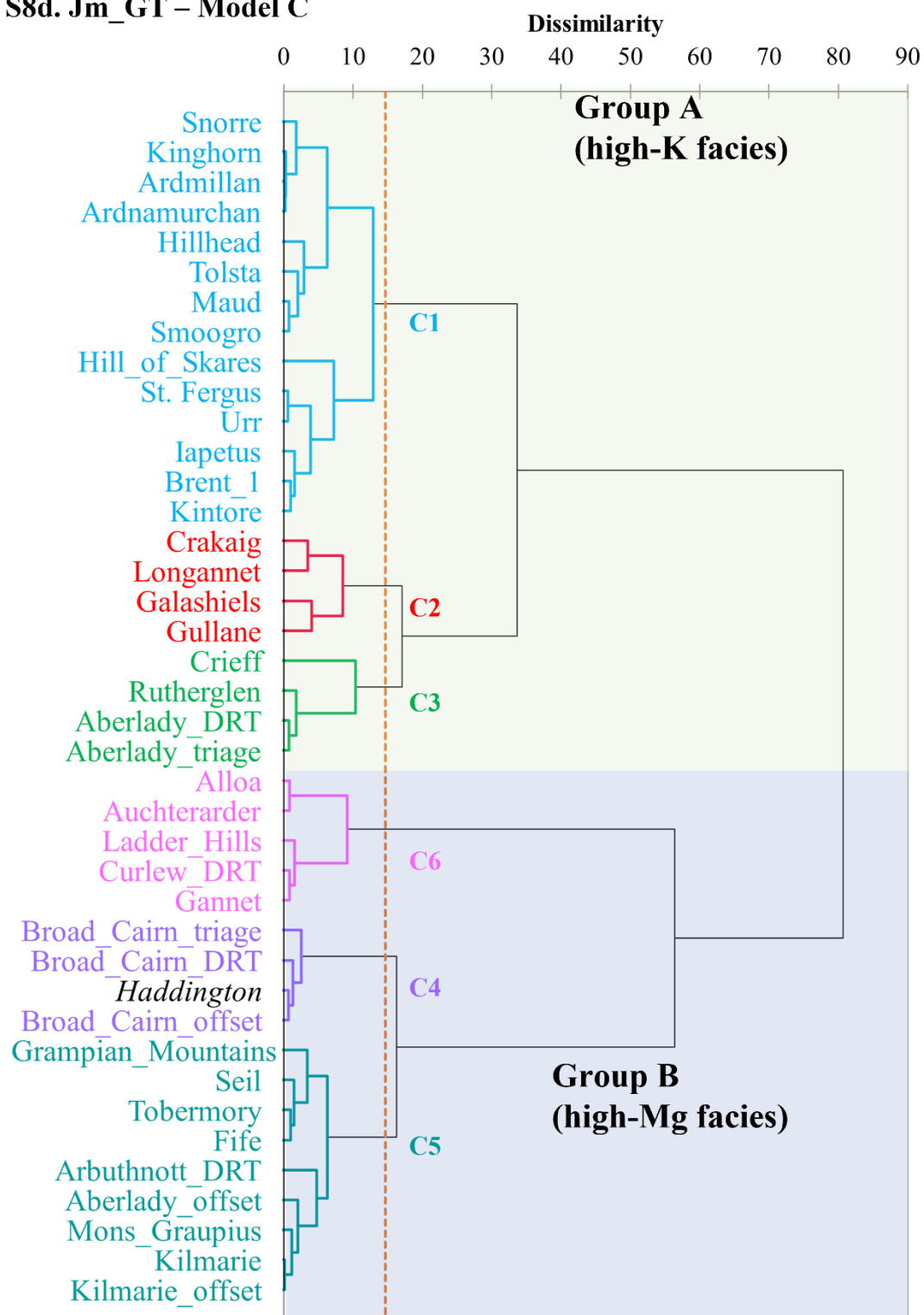
S8b. Jura_GT - Model A

Dissimilarity

Group A (high-K facies)

Group B (high-Mg facies)

C1, C2, C3, C4, C5, C6

14

S8c. Jura_GT - Model B

S8d. Jm_GT – Model C

a. PCA: Jm_GT AHCA Model A (axes F1 and F2: 59.79 %)

b. % Change in mean concentration, AHCA-derived clusters, relative to Mf+CSf
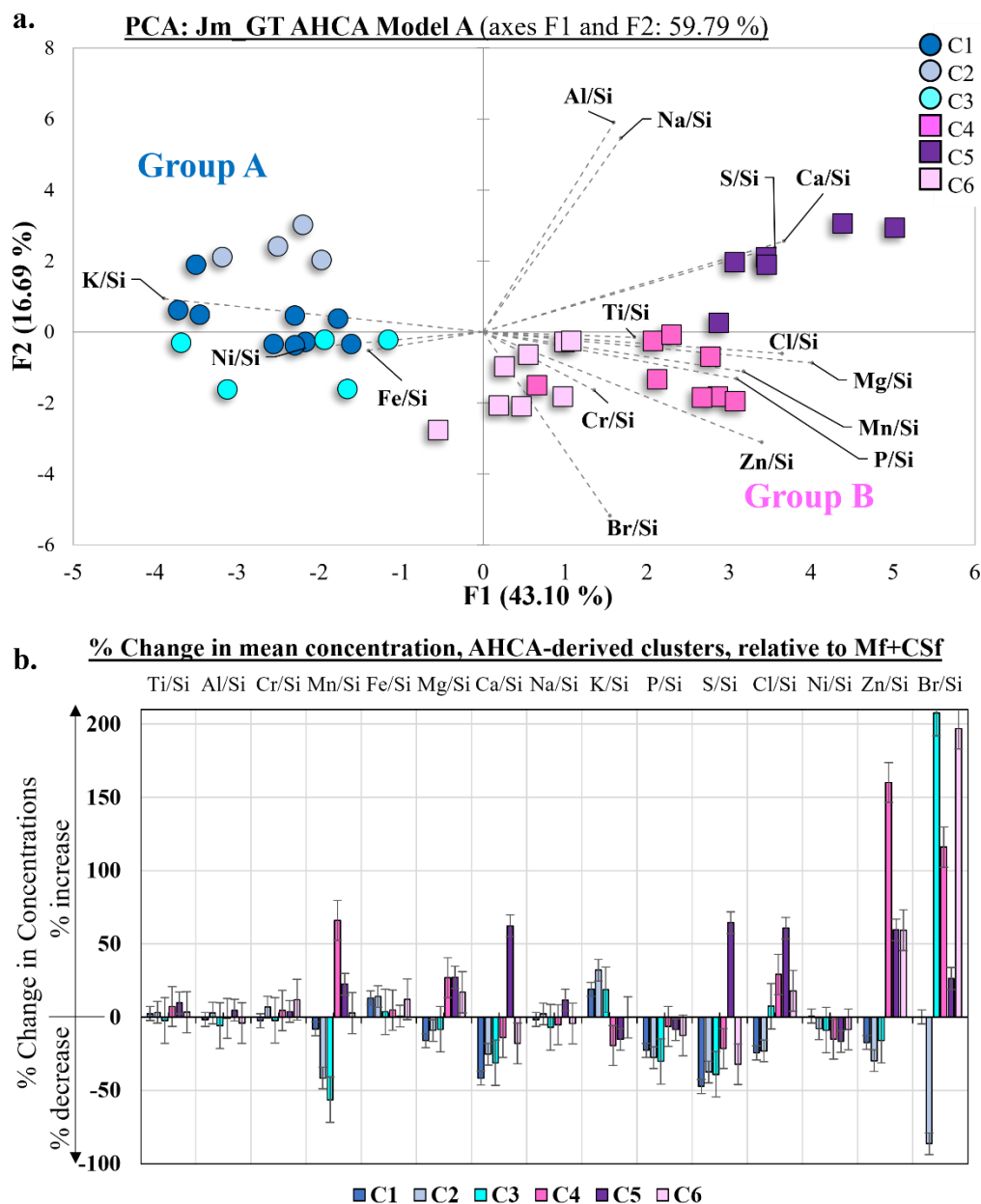
Figure S9. S9a. Multivariate Principal component analysis (PCA) of the Jura member, Glen Torridon (Jm_GT), using AHCA derived clusters (Model A parameters, K=6) using Log10 (element/Si) (mole/ratios) (Table S5a; Section 4.1.2). **S9b.** Percentage change in mean concentrations for Model A clusters (Table S5a), relative to mean Murray and Carolyn Shoemaker formations (Mf+CSf) (Table S1), calculated using mean element/Si (mole/ratios) for each cluster.

17

S10a. AHCA parameters for all models:
Clusters (K):   Six
Targets: Knockfarril Hill member – bedrock targets
Distance metric: Euclidean distance
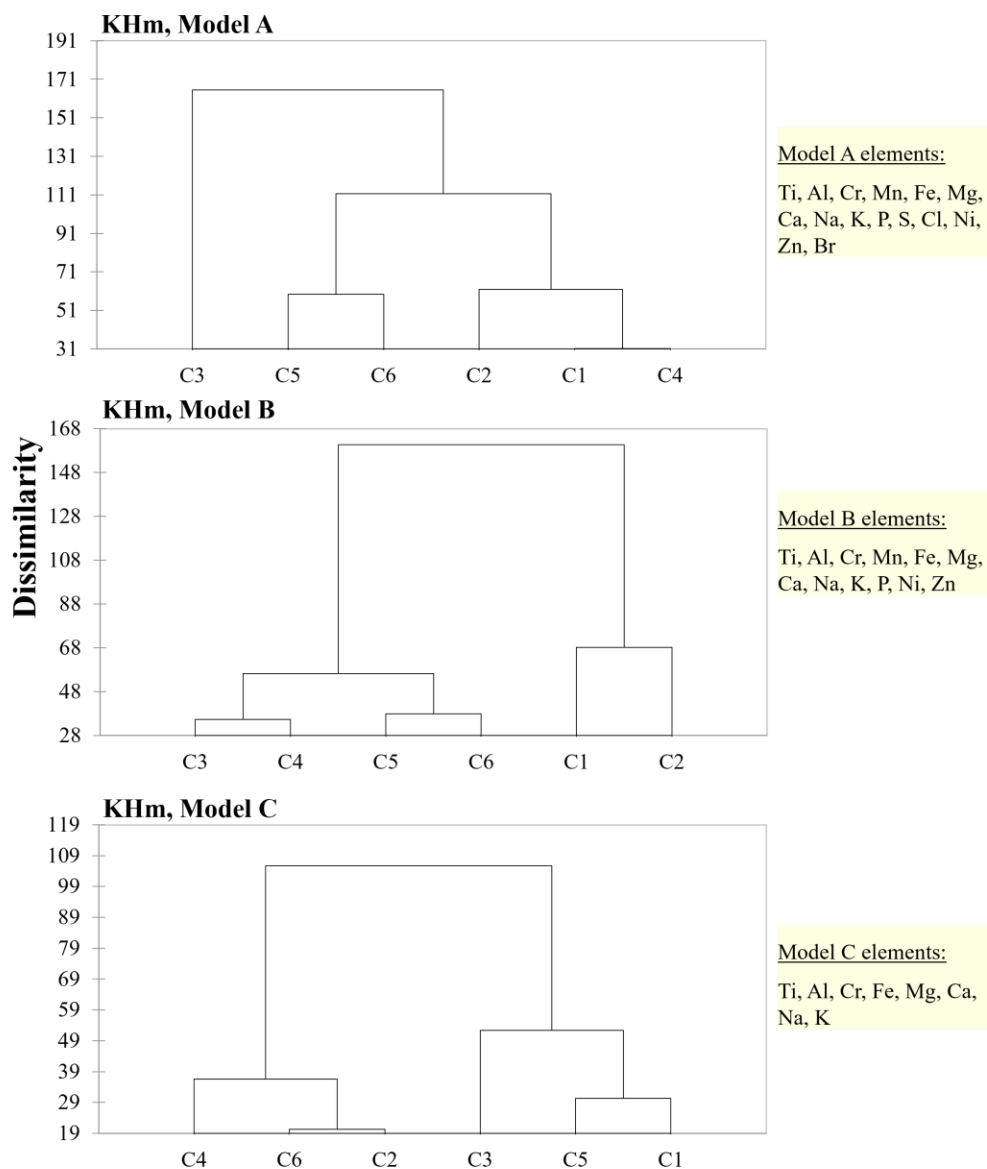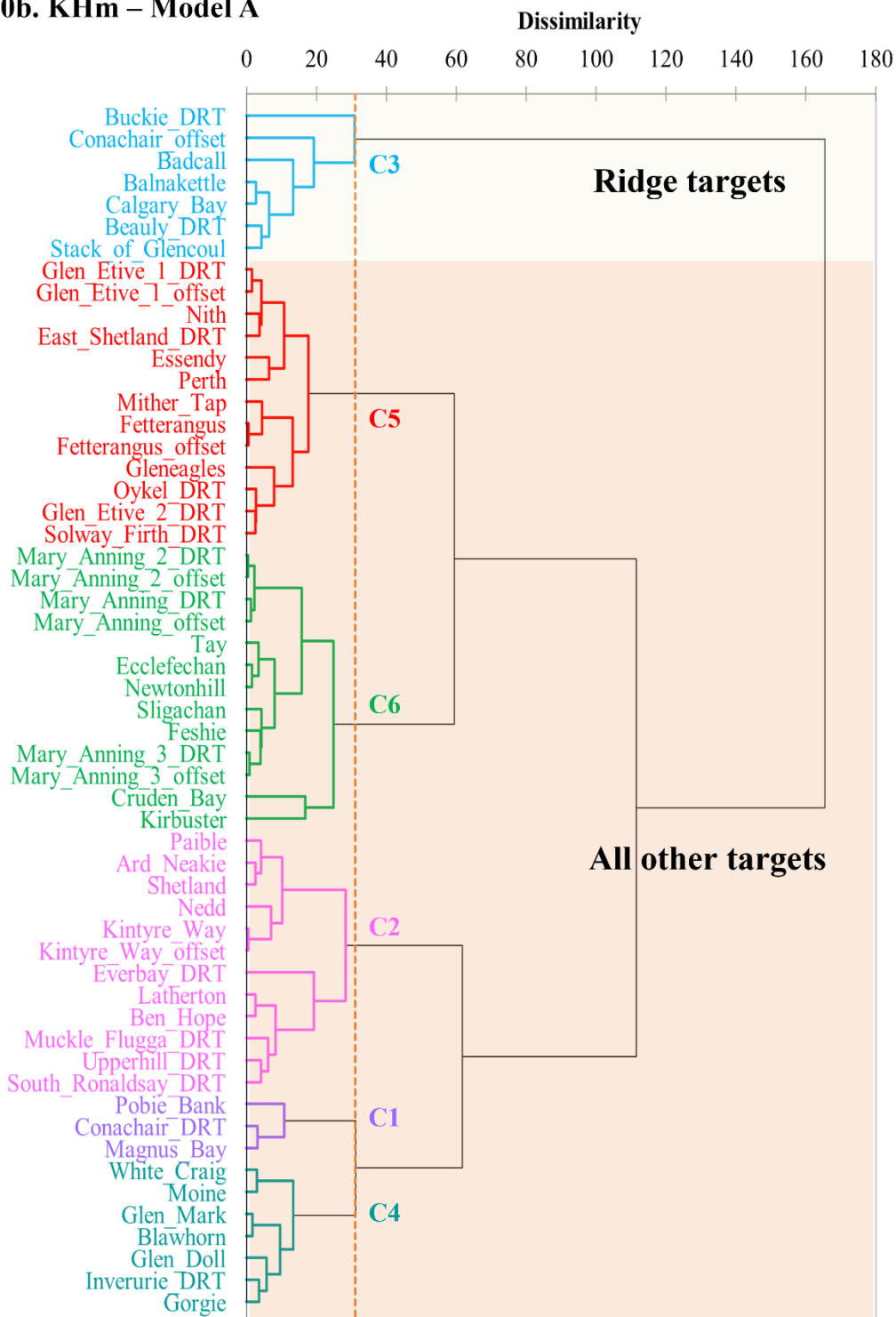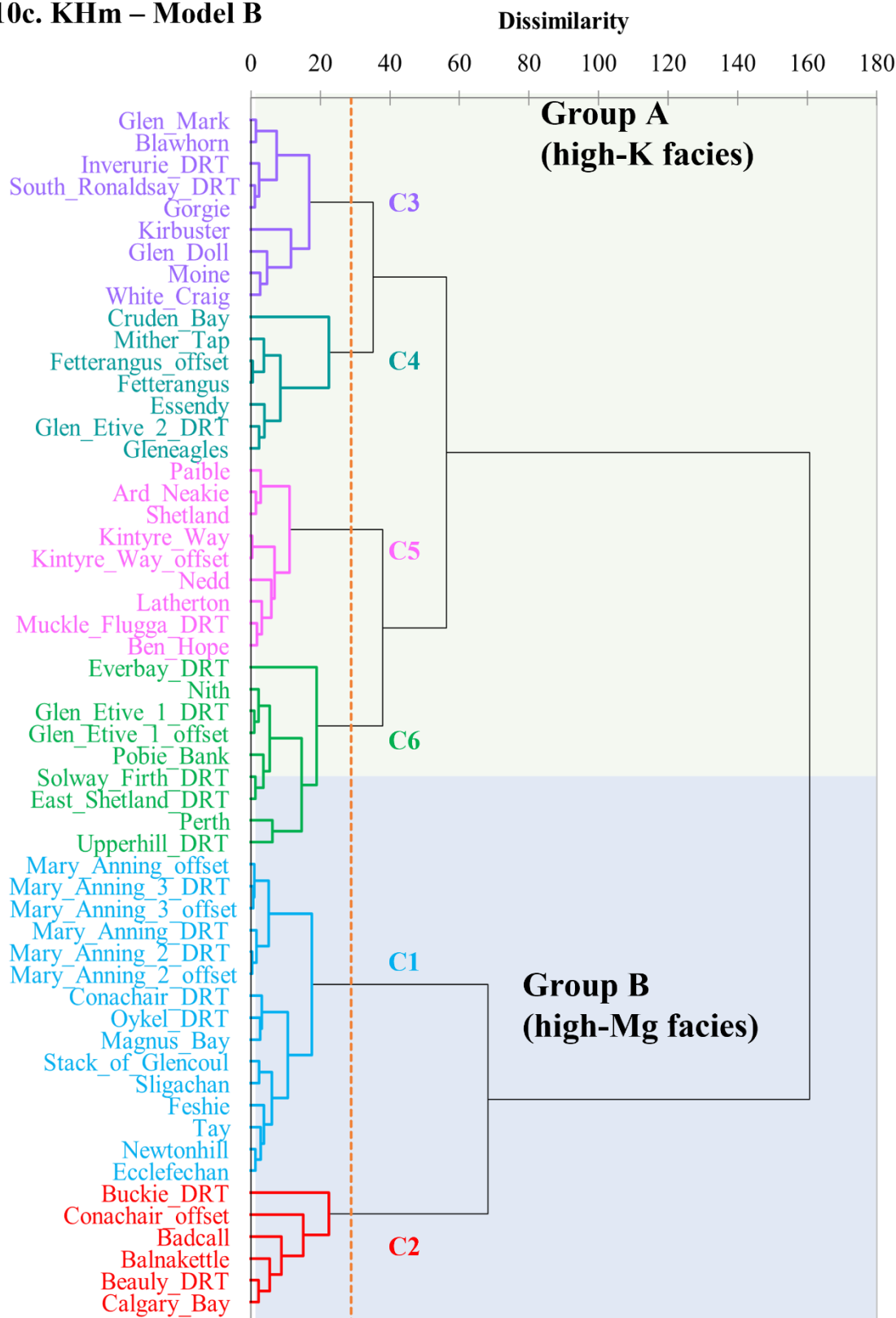Agglomeration method: Ward's method (Ward's minimum variance)

KHm, Model A

Model A elements:

Ti, Al, Cr, Mn, Fe, Mg, Ca, Na, K, P, S, Cl, Ni, Zn, Br

KHm, Model B

Model B elements:

Ti, Al, Cr, Mn, Fe, Mg, Ca, Na, K, P, Ni, Zn

KHm, Model C

Model C elements:

Ti, Al, Cr, Fe, Mg, Ca, Na, K

Figure S10. Agglomerative Hierarchical Clustering analysis (AHCA) dendrograms for the Knockfarril Hill member (Glen Torridon) (n targets = 55). All models were run using Log10 (element/Si) (mole ratios). Model parameters are discussed in Section 3.3 and Supplementary Text S2b; results are listed in Table S6a and discussed in Section 4.2.2. **S10a.** Comparison of dendrograms for Models A-C, with detailed views for each model (with target names in figures **S10b-S10d**.
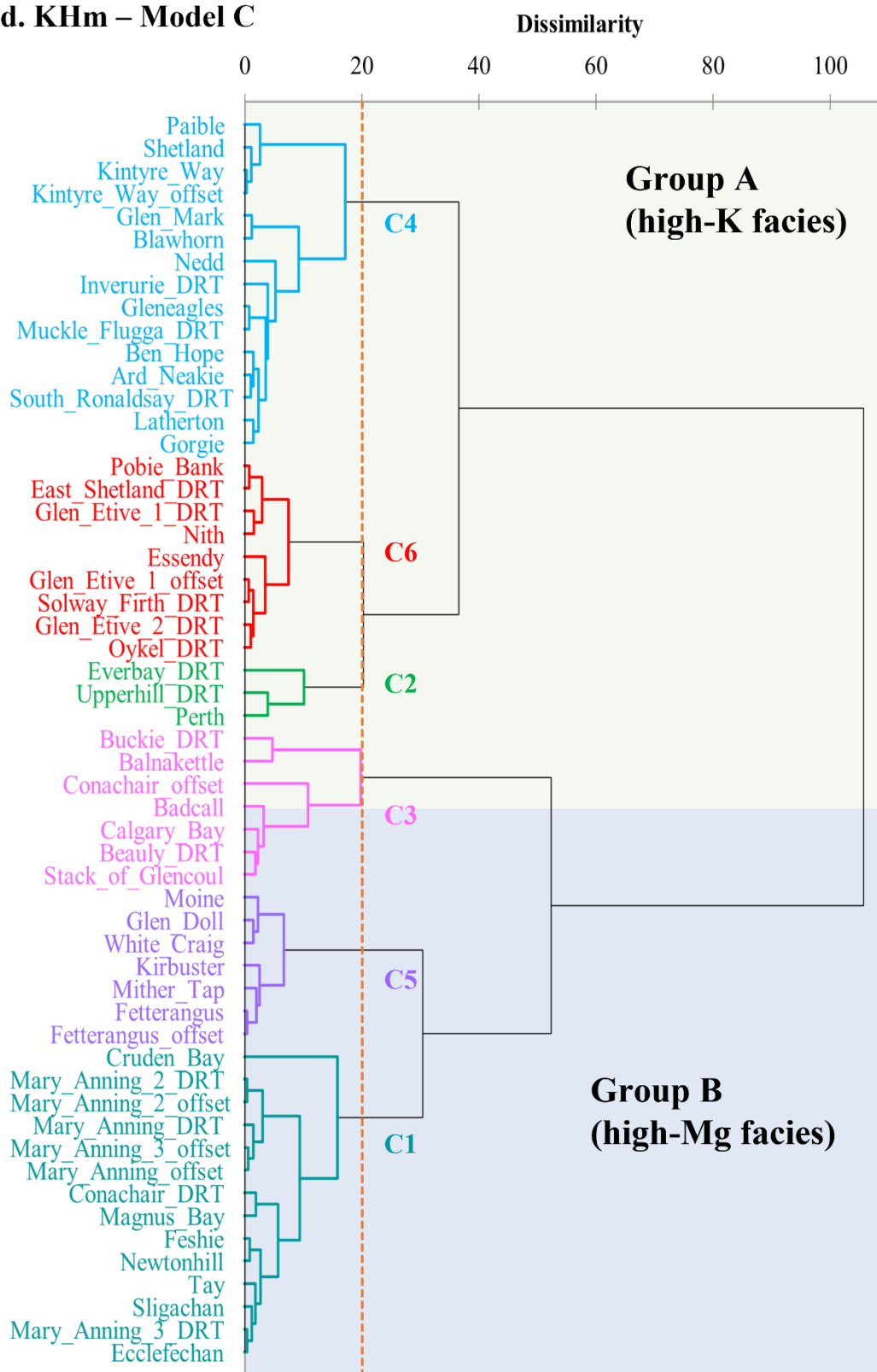
S10b. KHm – Model A

Dissimilarity

Ridge targets

All other targets

S10c. KHm – Model B

S10d. KHm – Model C

Dissimilarity

Group A (high-K facies)

Group B (high-Mg facies)

C4, C6, C2, C3, C5, C1

Paible, Shetland, Kintyre_Way, Kintyre_Way_offset, Glen_Mark, Blawhorn, Nedd, Inverurie_DRT, Gleneagles, Muckle_Flugga_DRT, Ben_Hope, Ard_Neakie, South_Ronaldsay_DRT, Latherton, Gorgie, Pobie_Bank, East_Shetland_DRT, Glen_Etive_1_DRT, Nith, Essendy, Glen_Etive_1_offset, Solway_Firth_DRT, Glen_Etive_2_DRT, Oykel_DRT, Everbay_DRT, Upperhill_DRT, Perth, Buckie_DRT, Balnakettle, Conachair_offset, Badcall, Calgary_Bay, Beauly_DRT, Stack_of_Glencoul, Moine, Glen_Doll, White_Craig, Kirbuster, Mither_Tap, Fetterangus, Fetterangus_offset, Cruden_Bay, Mary_Anning_2_DRT, Mary_Anning_2_offset, Mary_Anning_DRT, Mary_Anning_3_offset, Mary_Anning_offset, Conachair_DRT, Magnus_Bay, Feshie, Newtonhill, Tay, Sligachan, Mary_Anning_3_DRT, Ecclefechan

21

AHCA parameters for all models:
Clusters (K):   Seven
Targets: Glasgow (Gm) – bedrock targets
Distance metric: Euclidean distance
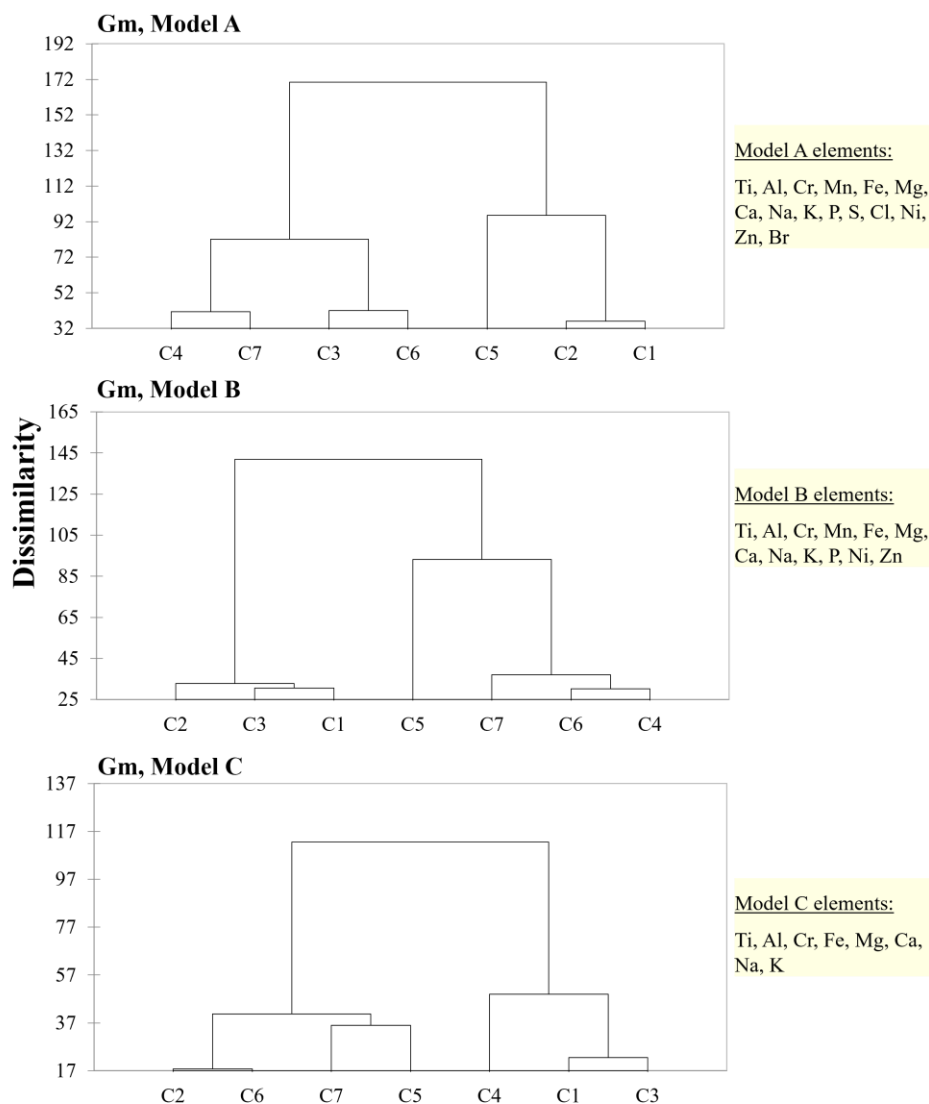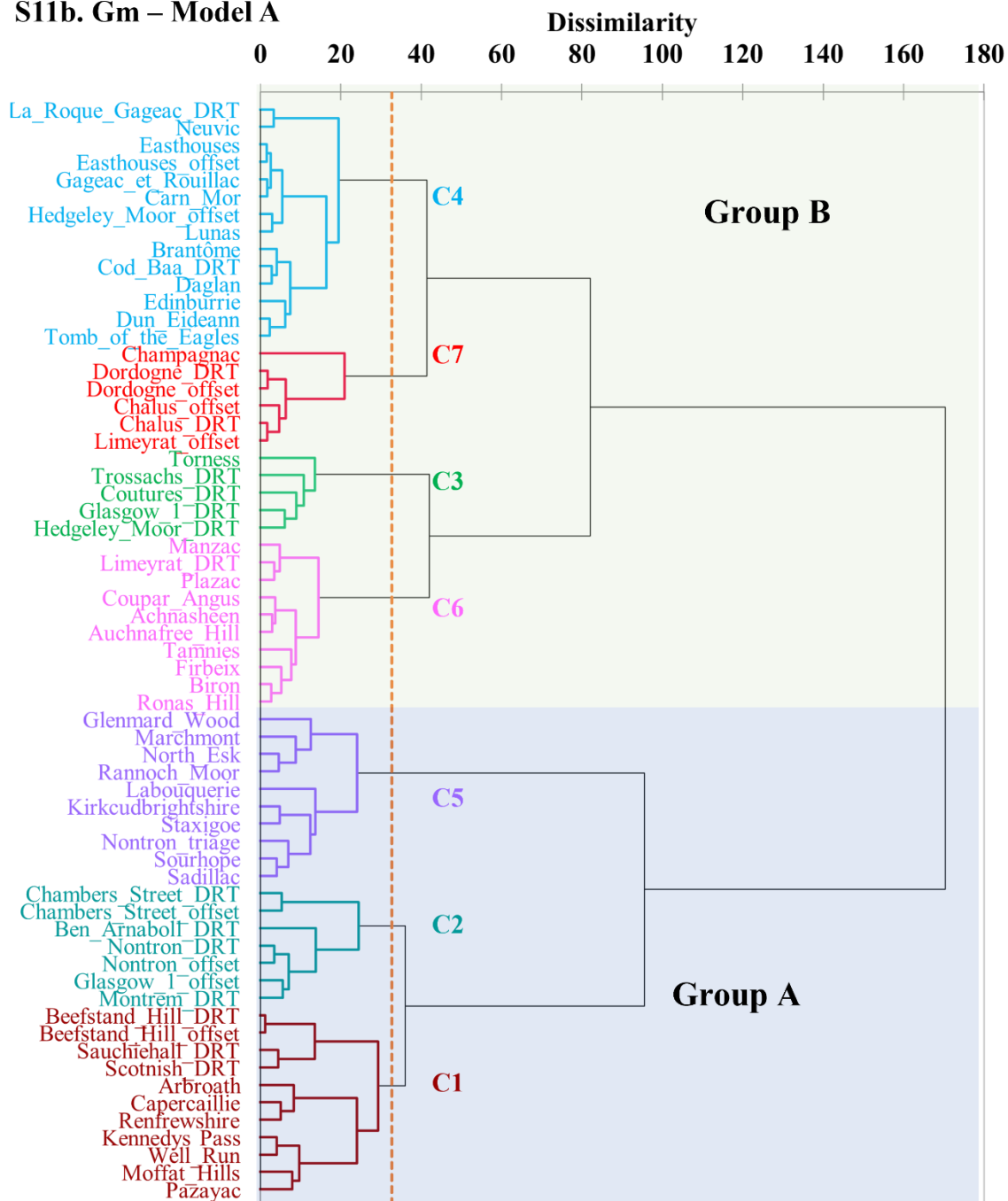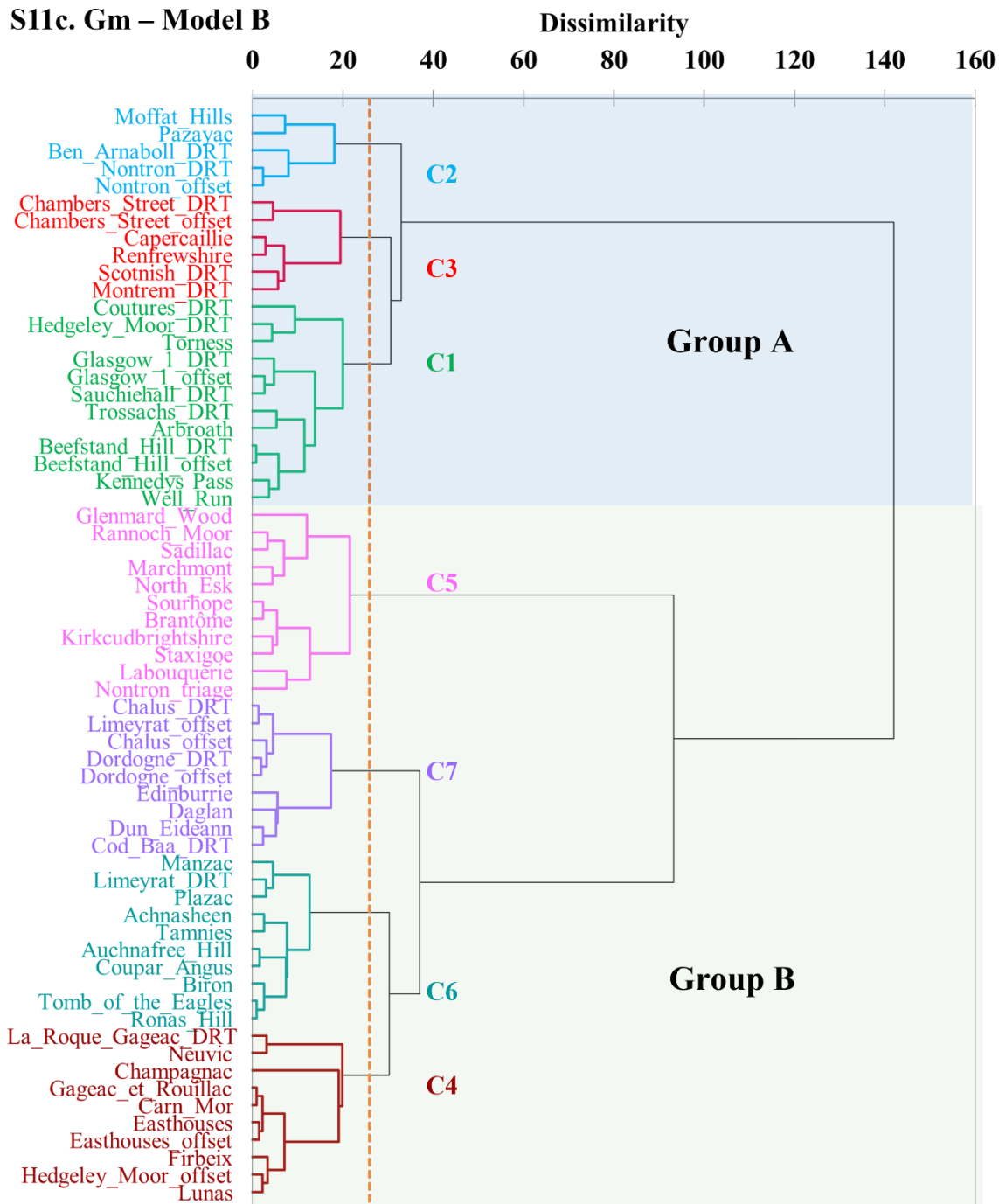Agglomeration method: Ward's method (Ward's minimum variance)

Gm, Model A

Model A elements:

Ti, Al, Cr, Mn, Fe, Mg, Ca, Na, K, P, S, Cl, Ni, Zn, Br

Gm, Model B

Model B elements:

Ti, Al, Cr, Mn, Fe, Mg, Ca, Na, K, P, Ni, Zn

Gm, Model C

Model C elements:

Ti, Al, Cr, Fe, Mg, Ca, Na, K

Figure S11. Agglomerative Hierarchical Clustering analysis (AHCA) dendrograms for the Glasgow member (Glen Torridon) (n targets = 63). All models were run using Log10 (element/Si) (mole ratios). Model parameters are discussed in Section 3.3 and Supplementary Text S2b; results are listed in Table S7a and discussed in Section 4.3.2. **S11a.** Comparison of dendrograms for Models A-C, with detailed views for each model (with target names in figures **S11b-S11d**).
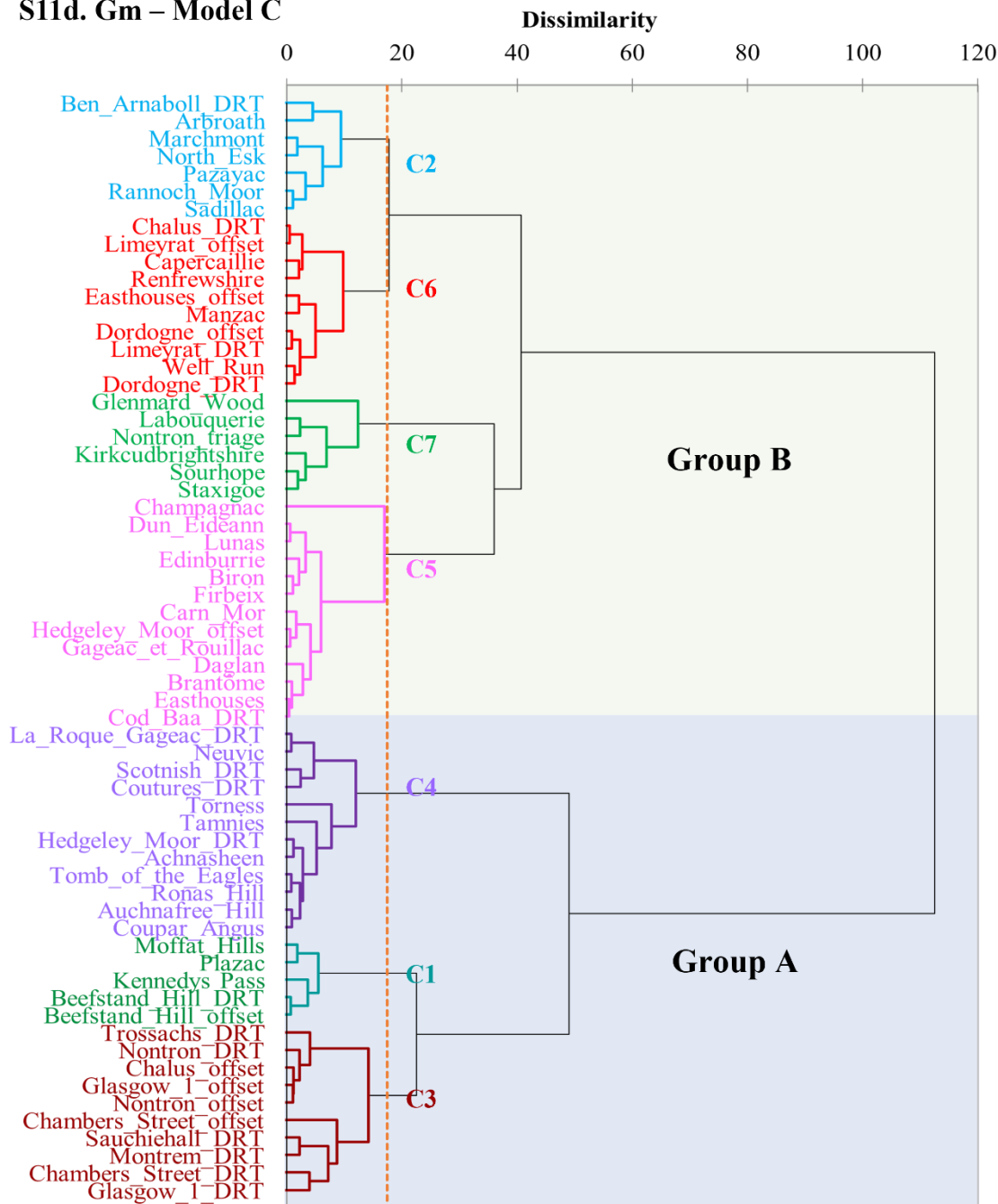
S11b. Gm – Model A

S11c. Gm – Model B

S11d. Gm – Model C

<

Tables S1-7 are uploaded separately as a single Excel file.

Table S1. APXS compositional data for all targets, including location information, errors and opearational statistics

Table S2. S2. Mean values for Glen Torridon subunits and facies, as defined in O'Connell-Cooper et al., 2022. All data (except Si molar) in element/Si (molar) form. Bedrock targets only included in mean analysis. Fines and diagenetic features (e.g., veins, nodules) are excluded.

Table S3. Pearson correlation coeffience (r), univariate analysis for all data. See Table S1 for full compositional data for targets within a given unit.

Table S4. Variance analysis, incorporating all targets included in mean Murray and Carolyn Shoemaker formations (i.e., mean Mf+CSf). Supplementary text S2a. for further details.

Table S5. Jura member (GT and VRR) subunit divisions, AHCA and variance analysis results. Element/Si (molar) concentrations in Table S1.

Table S6. Knockfarrill Hill member subunit divisions, AHCA and variance analysis results. Element/Si (molar) concentrations in Table S1.

Table S7. Glasgow member subunit divisions, AHCA and variance analysis results. Element/Si (molar) concentrations in Table S1.